# The feasibility of using an $L_1$ positioned dust cloud as a method of space-based geoengineering

R. Bewick[a,*], J.P. Sanchez[a], C.R. McInnes[a]

[a] *Advanced Space Concepts Laboratory, University of Strathclyde, 75 Montrose Street, Glasgow, UK, G1 1XJ*

**Abstract**

In this paper a method of geoengineering is proposed involving clouds of dust placed in the vicinity of the $L_1$ point as an alternative to the use of thin film reflectors. The aim of this scheme is to reduce the manufacturing requirement for space-based geoengineering. It has been concluded that the mass requirement for a cloud placed at the classical $L_1$ point, to create an average solar insolation reduction of 1.7%, is 7.60x$10^{10}$ kg $yr^{-1}$ whilst a cloud placed at a displaced equilibrium point created by the inclusion of the effect of solar radiation pressure is 1.87x$10^{10}$ kg $yr^{-1}$. These mass ejection rates are considerably less than the mass required in other unprocessed dust cloud methods proposed and are comparable to thin film reflector geoengineering requirements. Importantly, unprocessed dust sourced in-situ is seen as an attractive scheme compared to highly engineered thin film reflectors. It is envisaged that the required mass of dust can be extracted from captured near Earth asteroids, whilst stabilised in the required position using the impulse provided by solar collectors or mass drivers used to eject material from the asteroid surface.

*Keywords:*
geoengineering, dust cloud, lagrange point, three-body problem

## 1. Introduction

The current consensus within the scientific community is that climate change is not only happening but is almost unavoidable. Projections made using climate models over recent years have suggested that the mean global temperature is likely to increase by 1.1-6.4°C by the end of this century (IPCC, 2007). With the continuing industrialisation of the developing world and the lack of an agreed international protocol on tackling of greenhouse gas emissions, this temperature increase seems unstoppable. While the focus of international efforts should remain with the attempts to prevent climate change by the reduction of greenhouse gas emissions, it is prudent to investigate methods to mitigate its effects. This can be achieved by the deliberate manipulation of the Earth's climate, commonly referred to as climate engineering or geoengineering.

Several proposals for possible geoengineering methods have been made and these can generally be placed in two categories; solar radiation management and carbon sequestration (Royal Society, 2009). Solar radiation management focuses on the reduction of the amount of sunlight being absorbed by the Earth's atmosphere by either increasing the Earth's albedo, for example through using more reflective roofing materials, or by reducing the level of sunlight reaching the surface, for example by placing aerosol particles into the stratosphere to reflect sunlight. Alternatively carbon capture techniques aim to deal with the fundamental cause of global warming by either direct or indirect methods. Direct methods include schemes such as capturing $CO_2$ from the air and placing it into storage, whilst an example of an indirect method is the fertilisation of the ocean to stimulate increased algal growth with these algae then leading to increased $CO_2$ uptake.

A report into geoengineering conducted by the Royal Society in 2009 (Royal Society, 2009) examines the feasibility of all types of schemes based on the criteria of effectiveness, affordability, timeliness and safety. In general the report appears to show that there is no perfect solution with the schemes that appear most effective suffering in other criteria such as affordability. One of the most effective solutions suggested is the use of space-based solar reflectors to reduce incident solar insolation. Whilst this technique does not appear to be affordable or timely, it does have a key advantage over other schemes; neither the Earth's surface nor atmosphere needs to be physically changed.

This is a significant benefit as it reduces the grounds for ethical objections based on the risky nature of many geoengineering proposals. As an example, the injection of $SO_2$ particles into the stratosphere is rated as having low safety in the Royal Society report. This is because there are indications, from observations of volcanic eruptions, that an increased sulphate concentration in the stratosphere could have adverse effects on the hydrological cycle and ozone

*Corresponding author
*Email addresses:* russell.bewick@strath.ac.uk (R. Bewick), jpau.sanchez@strath.ac.uk (J.P. Sanchez), colin.mcinnes@strath.ac.uk (C.R. McInnes)

layers (Royal Society, 2009). Space-based geoengineering will avoid the risks associated with these types of schemes though there may yet be side effects that cannot be predicted.

It has been estimated that in order to offset the effects of global warming caused by a doubling of the $CO_2$ concentration (compared to pre-industrial levels and corresponding to an increase in global temperature of approximately 2°C) solar insolation must be reduced by 1.7% (Govindasamy and Caldeira, 2000). Similarly for a quadrupling of $CO_2$ the required insolation change is 3.6% (Govindasamy et al., 2003).

There have been several different proposals to date regarding the reduction of solar insolation using space-based methods the key characteristics of which can be seen in Table 1. The methods either utilise a cloud of dust (Pearson et al., 2006; Struck, 2007) or solid reflectors or refractors (Pearson et al., 2006; McInnes, 2010; Early, 1989; Mautner, 1991; Angel, 2006) to reduce the level of solar insolation. Typically the methods that require the least mass are those that use solid reflectors/refractors whilst the mass for dust cloud methods are orders of magnitude higher. This is mostly due to the increased level of control that can be placed upon the solid reflectors, hence they can be stationed in optimum positions. Dust clouds cannot be controlled and can only be placed with suitable initial conditions, with subsequent replenishment necessary due to the orbital decay or perturbation of the particle orbits. Conflicting with this, though, is the consideration of the engineering complexity of the system. Whilst dust clouds are a relatively crude method, the material can be readily produced with little processing required, whereas solid reflectors must either be manufactured terrestrially and then launched into position or manufactured in-situ. Clearly taking this into account, the low rating for affordability and timeliness indicated in the Royal Society report can be understood.

The method proposed in (Pearson et al., 2006) to place a ring of dust or reflecting satellites in Earth orbit, though comparatively low in mass, clearly has possible side effects including an increased danger to Earth orbiting satellites. Additionally the ring will have the effect of increasing reflected light onto the night side of the Earth under certain conditions. For these reasons this method is not seen as the most optimal space-based geoengineering solution.

An additional factor that affects the relative mass of the different methods is the amount of time that the reflectors spend along the Sun-Earth line. For example the method proposed in (Struck, 2007) to place clouds of dust at the $L_4/L_5$ Lagrange libration points of the Earth-Moon system has a clear benefit as these points are passively stable. However, as these points effectively orbit around the Earth they are only occasionally in a position to reduce solar insolation. Furthermore, the movement of the clouds will create a flickering effect. On most occasions there will be no change in insolation whilst at those times when the cloud is present the insolation change required will be much greater than the net 1.7% reduction.

Ultimately none of these concepts are ideal for geoengineering, though should the technology become available and the necessity to act quickly on climate change become apparent they could still be implemented. The aim of this paper is to propose a space-based geoengineering concept that reduces the manufacturing requirement, thus improving the affordability and timeliness of this method of geoengineering, by placing clouds of dust at the Sun-Earth $L_1$ point. An example of this concept can be seen in Fig. 1.

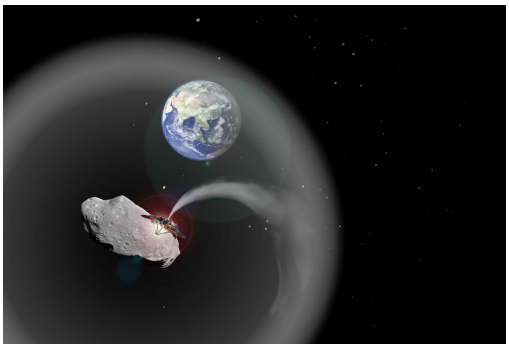

Figure 1: Impression of an $L_1$ positioned dust cloud for space-based geoengineering.

The feasibility of this method shall be explored by first investigating the dynamics of material at the $L_1$ point. It is well known that the $L_1$ point is unstable, but it is none-the-less an equilibrium point where particles could remain for a significant period of time given appropriate initial conditions. Therefore, this paper will use an analysis of the stability properties of the $L_1$ point to make an estimate of the average lifetime of a dust cloud with different cloud radii, different sizes of dust grains and their initial conditions. The optimum initial conditions of the cloud can then be found to maximise the net insolation reduction.

Subsequently, the ability of the cloud to reduce solar insolation will be investigated. This will be achieved by means of a solar radiation model (SRM). The model will initially be used to determine the characteristics of the cloud that most efficiently creates the required reduction in solar insolation. The variables in this case will be the cloud size as well as the grain radius and number density. Subsequently the SRM will be used to analyse the ability of the optimum dust cloud to reduce solar insolation.

## 2. Dust Dynamics

The following section will detail the dynamics of a dust cloud in the vicinity of the interior Lagrange point in the Sun-Earth three-body problem.

### *2.1. Three-body problem*

The cloud shall be assumed to be moving in a system where only the gravitational forces due to the Sun and

| Position | Method | Insolation Change [%] | Required Mass [kg] | Estimated Energy [J] | Reference |
|---|---|---|---|---|---|
| Earth orbit | Dust ring | 1.6 | $2.3 \times 10^{12}$ | $2.4\times10^{19}$ -$1.0\times10^{21}$ | (Pearson et al., 2006) |
| Earth orbit | Solar Reflector | 1.6 | $5.0 \times 10^{9}$ | $2.0 \times 10^{18}$ | (Pearson et al., 2006) |
| Earth-Moon $L_4/L_5$ | Dust cloud | 1.4 | $2.1 \times 10^{14}$ | $2.2 \times 10^{20}$ -$4.6 \times 10^{21}$ | (Struck, 2007) |
| Sun-Earth $L_1$ | Solar reflector | 1.8 | $2.6 \times 10^{11}$ | $1.8 \times 10^{20}$ | (McInnes, 2010) |
| Sun-Earth $L_1$ | Solar refractor | 1.8 | $2.0 \times 10^{10}$ | $1.3 \times 10^{19}$ | (Angel, 2006) |
| Sun-Earth $L_1$ | Dust cloud (10 yr duration) | 1.7 | $1.9 \times 10^{11}$ | $1.5 \times 10^{17}$ | This paper |

Table 1: The key characteristics of proposed space-based geoengineering schemes to offset global warming.

the Earth are significant. Hence, the circular restricted three-body problem (CR3BP) shall be used to describe the motion of the dust particles in the cloud. The dimensionless equations of motion in a rotating reference frame are given by;

$$\begin{aligned} \ddot{x} - 2\dot{y} &= \frac{\partial U}{\partial x} \\ \ddot{y} + 2\dot{x} &= \frac{\partial U}{\partial y} \\ \ddot{z} &= \frac{\partial U}{\partial z} \end{aligned} \tag{1}$$

where the non-dimensional potential function, $U$, is;

$$U(x,y,z) = \frac{1}{2}\left(x^2+y^2\right) + \frac{1-\mu}{\rho_1(x,y,z)} + \frac{\mu}{\rho_2(x,y,z)} \tag{2}$$

Here the mass ratio of the secondary to total system mass is $\mu = M_2/(M_1+M_2)$ and the parameters $\rho_{1,2}$ are the distances of the particle to each of the primary and secondary masses, Eq. (3) and Eq. (4), as shown in Fig. 2. In dimensionless co-ordinates the Sun and Earth are positioned at $M_1(-\mu,0,0)$ and $M_2(1-\mu,0,0)$ respectively. Hence;

$$\rho_1 = \sqrt{(x+\mu)^2+y^2+z^2} \tag{3}$$

$$\rho_2 = \sqrt{(x+\mu-1)^2+y^2+z^2} \tag{4}$$

The equilibrium, or libration points, are located where the combined gravitational force of the two primary bodies on a particle is equal to the centripetal force required for it to orbit in a fixed position relative to the two primary bodies. These positions can be found by finding the stationary points of the potential function, Eq. (2). In particular, the equilibrium points required for this geoengineering method must lie along the Sun-Earth line and must therefore be along the $x$ axis hence $y = z = 0$. Using this, and substituting Eq. (2) into Eq. (1), results in Eq. (5), with which the position of the $L_1$ point, $x_{L_1}$, can be found numerically;

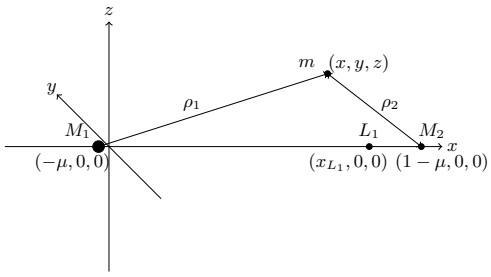


Figure 2: Geometry of the circular restricted three-body problem with the Sun, $M_1$, Earth. $M_2$ and dust grain $m$.

$$x_{L_1} - \frac{1-\mu}{(x_{L_1}+\mu)^2} + \frac{\mu}{(x_{L_1}+\mu-1)^2} = 0 \tag{5}$$

For the Sun-Earth system the $L_1$ point is located approximately $1.5 \times 10^6$ km from the Earth.

### *2.2. Perturbation forces*

Due to the small scale of the dust particles used in this study the effects of natural perturbation forces must be analysed to determine whether they will greatly effect the motion of the dust grains. The perturbations to be analysed are due to solar radiation pressure, the Poynting-Robertson effect, interactions with the solar wind and the Lorentz force.

*2.2.1. Solar Radiation Pressure*

The effects of solar radiation pressure (SRP) will be discussed more thoroughly in Sec. 2.3. This effect is caused by the transfer of momentum from solar photons to the dust grain and the force can be approximated as follows (de Pater and Lissauer, 2001);

$$F_{SRP} = \frac{L_\odot \sigma_{gr} Q}{4\pi c r_\odot^2} \tag{6}$$

where $L_\odot$ is the solar luminosity, $\sigma_{gr}$ is the grain cross-sectional area, $c$ is the speed of light, $r_\odot$ is the distance to the Sun and $Q$ is the radiation pressure coefficient. The parameter $Q$ determines the coupling effect of SRP and is dependent upon the material of the dust grain. For example, a completely transparent material will have a value of $Q = 0$ whilst for a completely absorbing grain $Q = 1$ and for a completely reflecting grain $Q = 2$. The values of $Q$ that shall be used to calculate $F_{SRP}$ for a range of particles are interpreted from a study by (Wilck and Mann, 1996) on the effect of SRP on interplanetary silicate grains where $\rho = 3,500 \mathrm{kg\,m^{-3}}$. The study shows a peak for $Q$ in the range where the grain size is approximately equal to the wavelength of visible light. Analysing Eq. 6 shows that as the grain size decreases the acceleration experienced by a grain increases due to the greater area-to-mass ratio.

*2.2.2. Poynting-Robertson Effect*

This perturbation is due to the motion of a dust grain with respect to the stream of solar photons. Firstly, the Doppler shift of sunlight due to the grains velocity in the radial direction, and secondly the motion of the grain causes solar photons to be incident from a slightly forward direction. The resultant force due to the Poynting-Robertson (PR) effect can be found as follows (de Pater and Lissauer, 2001);

$$F_{PR} = F_{SRP}\left(\frac{-2v_r}{c}\hat{\mathbf{r}}, \frac{-v_\theta}{c}\hat{\theta}\right) \tag{7}$$

where $c$ is the speed of light, $v_r$ is the radial velocity and $v_\theta$ is the transverse velocity in the directions $\hat{r}$ and $\hat{\theta}$ respectively. Thus there will be a drag force acting against the velocity vector of the grain.

*2.2.3. Solar Wind*

The effect that the solar wind has on a dust grain is much the same in principle to the Poynting-Robertson effect, the difference being that the momentum transfer is due to protons, eletrons and helium nuclei in the solar wind striking the dust grain. The force due to the solar wind can thus be found to be (Minato et al., 2004);

$$F_{sw} = p_{sw}\left(1 - \frac{-2v_r}{v_{sw}}\hat{\mathbf{r}}, \frac{-v_\theta}{v_{sw}}\hat{\theta}\right) \tag{8}$$

where $v_{sw}$ is the speed of the solar wind and $p_{sw}$ is the momentum transfer to the grain defined by;

$$p_{sw} = \frac{2E_{sw}\Omega_{sw}A_{gr}C_{sw}}{v_{sw}} \tag{9}$$

Here $E_{sw}$ is the average energy of a solar wind particle, $\Omega_{sw}$ is the flux of solar wind particles, $A_{gr}$ the cross-sectional area of the grain and $C_{sw}$ is the momentum transfer coefficient. The value of $C_{sw}$ is close to unity for grain radii $> 0.1\,\mu$m decreasing significantly below this due to the "small particle effect" (Minato et al., 2004).

The solar wind can be considered to have two states, the fast solar wind and the quiet solar wind. During the slow phase the velocity of particles is typically 300-500 $\mathrm{km\,s^{-1}}$ with a proton density in the range of 5-8 $\mathrm{cm^{-3}}$. In contrast the fast solar wind will have a typical velocity of 500-900 $\mathrm{km\,s^{-1}}$ and a proton density of 8-12 $\mathrm{cm^{-3}}$ (de Pater and Lissauer, 2001). The number density of $\alpha$-particles for the fast and quiet solar winds are typically 2-4% (Kellenrode, 2004) and thus for an initial estimate they can be ignored. For the case of a Coronal Mass Ejection, where the solar wind velocity is typically 400-2,000 $\mathrm{km\,s^{-1}}$ this percentage rises to approximately 30% (Kellenrode, 2004), thus in this scenario their greater mass must be taken into account.

*2.2.4. Lorentz Force*

The Lorentz force perturbation is due to the motion of a charged grain through the solar magnetic field. The direction of this force is defined by the cross product as seen in Eq. 10. The magnetic field of the Sun is carried out by the solar wind and forms a 3D structure, the "heliospheric current sheet" (Wagner, 2007), the shape of which is described as a Parker spiral.

$$F_L = q\mathbf{v} \times \mathbf{B} \tag{10}$$

The magnetic field is described in (de Pater and Lissauer, 2001) as having approximately equal radial and azimuthal components at the Earth's orbit with the strength being in the region of 0.3-1$\times 10^{-8}$ T for a quiet solar wind and 0.8-1.6$\times 10^{-8}$ T for the fast solar wind. Additionally the magnetic field switches polarity intermittenly, depending on the polarity of the region on the Sun's surface where the solar wind, found at a given position and time, originates.

An important factor that must be considered is the charge on the dust grain. This has been found to vary little with distance to the Sun (Kimura and Mann, 1998). For a silicate grain the surface potential was modelled to be $U_{gr} = 3.2$V at 1AU for a grain radius of 0.281$\mu$m. Above this particle size the surface charge does not vary, with only a marginal increase below. Thus, this surface potential shall be assumed to apply for all grain sizes. The charge on the grain can be found using;

$$q = 4\pi\epsilon_0 U_{gr} R_{gr} \tag{11}$$

where $\epsilon_0$ is the permittivity of free space and $R_{gr}$ is the grain radius. Subsequently the force on a grain can be found using Eq. 10. It should be noted that no assumptions are made regarding the charging timescale of the dust grain as a worst case scenario is sought to determine the effect of the perturbation forces.

### *2.2.5. Perturbation Summary*

To demonstrate the relative strengths of the different perturbations the acceleration on a range of dust grain sizes shall be calculated. The grain is assumed to be initially placed at the classical $L_1$ position and will thus have an orbital speed of approximately $30\,\mathrm{km\,s^{-1}}$ in the transverse direction. Using the equations described above and assuming the grain is spherical with a density of $3,500\mathrm{kg\,m^{-3}}$ the accelerations can be calculated, as seen in Fig. 3.

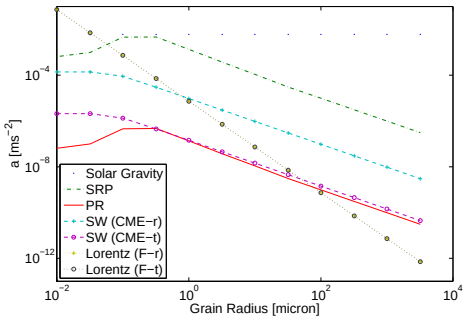


Figure 3: Acceleration due to solar radiation pressure (SRP), solar gravity, the Poynting-Robertson effect (PR), the solar wind (CME event)and the Lorentz force for a range of dust grain sizes for radial (-r) and transverse (-t) directions. For the solar wind and Lorentz force cases only the strongest acceleration scenario is plotted for clarity.

It can clearly be seen that above a radius of $0.06\,\mu$m the dominant perturbation is SRP, with only the Lorentz force being greater below this. This force decreases rapidly with grain radius becoming an order of magnitude lower than SRP for a grain radius of $0.1\,\mu$m. Following this investigation it can be concluded that above a grain radius of $0.1\,\mu$m only SRP needs to be taken into account. Therefore, only grain sizes above this limit will be considered from now on.

## *2.3. Effect of solar radiation pressure*

Generally the effect of SRP is relatively small due to the large area-to-mass ratio of conventional satellites. However, for dust particles this is not the case. Here the surface area-to-mass ratio is large and therefore a significant momentum transfer will take place between solar photons and the dust particles. The effect of SRP can be quantified using the 'lightness' parameter, $\beta$, which is the ratio of the force due to SRP and solar gravity (de Pater and Lissauer, 2001);

$$\beta = \left|\frac{F_{rad}}{F_g}\right| \approx 570\frac{Q}{\rho R_{gr}} \tag{12}$$

where $\rho$ [$\mathrm{kg\,m^{-3}}$] is the grain density and $R_{gr}$ [$\mu$m] is the radius of the grain.

For relatively large radius particles, $R_{gr} > 1\mu$m, the value of $Q$ varies little but as the size decreases the interaction between the solar photons and the dust grains becomes more complex.The $\beta$-value for a range of particle radii using Mie theory for different composition models is calculated in (Wilck and Mann, 1996). The results for a typical asteroidal dust grain can be seen in Fig. 4. This shows that the $\beta$-value peaks with a value of approximately 0.9 at a radius of $0.2\mu$m before decreasing to 0.1 for a radius of $0.01\mu$m. Also shown in Fig. 4 are lines relating the grain sizes that will be modelled, as will be described later, to their corresponding beta values.

Due to the nature of the SRP, the effect is to reduce the effective gravitational force of the Sun. Hence, the mass parameter, $\mu$, for the three-body problem is now;

$$\mu = \frac{M_2}{(1-\beta)M_1 + M_2} \tag{13}$$

Due to the increase in the value of $\mu$ with increased $\beta$ the $L_1$ equilibrium point is found to shift towards the Sun. The magnitude of this effect can be seen in Fig. 5. For particles with $\beta > 0$ placed at the conventional $L_1$ point this displacement from the equilibrium point will lead to a shorter instability timescale.

A possible beneficial effect of increased $\beta$ is that the gradient of the potential function, Eq. (2), will be reduced around the new equilibrium point in comparison to the classical $L_1$ point. This will lead to improved stability if the dust cloud is positioned at this point, though the effect that the dust cloud has on the solar insolation reduction is likely to be reduced as a smaller solid angle is subtended when viewed from the Earth.

It should be noted that it is assumed, for simplicity, that all particles within the cloud receive the same incident solar radiation. In reality this would not be the case as the attenuation of the solar photons would lead to a decreased value of $F_{SRP}$ for particles not at the Sun facing boundary of the cloud and hence the effect of SRP would reduce. The magnitude of this effect would vary depending on the size and level of insolation change required. For example a relatively small cloud may require a very large average attenuation of solar radiation and hence the particles at the Earth facing boundary are likely to have a much smaller $\beta$-value than expected. There may also be unforseen side-effects due to other factors, for example the self gravity of the cloud or collisions between the dust grains. For the cloud lifetimes associated with this scenario these factors should be small. A large potential source for error is the mechanism by which the cloud is generated, for example the initial velocity given to the particles. However these issues cannot be dealt with in this initial study.

## *2.4. Transition matrix*

Critical to this study is the ability to predict the motion of dust particles in relation to the $L_1$ point. This is

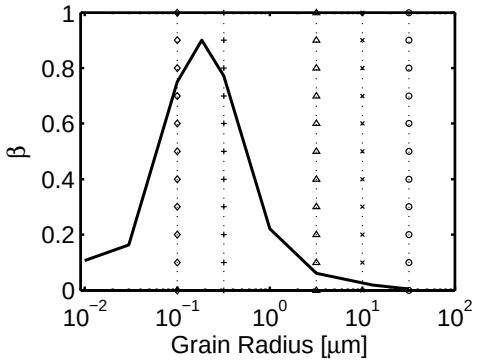


Figure 4: Variation in $\beta$ with particle radius for an asteroidal dust grain model as described in (Wilck and Mann, 1996). The coloured lines correspond to the mass requirement results shown later.

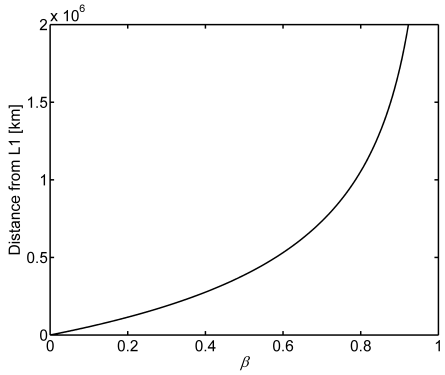


Figure 5: Sunward shift of the new equilibrium point, found when the effect of solar radiation pressure is included, in comparison to the conventional $L_1$ libration point.

because the libration point is unstable and therefore particles will naturally drift away if there is no control strategy implemented, as is the case for a passive dust cloud. The most efficient method for determining the motion of a large group of particles is to generate a transition matrix, $\Phi(t, t_0)$, which describes the motion of the cloud as a whole. This is in contrast to the method which propagates the equations of motion for each dust particle within the cloud individually. For predicting the motion of large groups of particles the transition matrix method is more computationally efficient and is sufficiently accurate for small time periods. The transition matrix maps the initial state vector, $X(t_0)$, of each single dust grain into the state vector $X(t)$, as in Eq. (14).

$$X(t) = \begin{bmatrix} x(t) \\ v(t) \end{bmatrix} = \Phi(t, t_0) X(t_0) \tag{14}$$

where the transition matrix, $\Phi(t, t_0)$, is defined by;

$$\Phi(t, t_0) = \begin{bmatrix} \frac{\partial x(t)}{\partial x(t_0)} & \frac{\partial x(t)}{\partial v(t_0)} \\ \frac{\partial v(t)}{\partial x(t_0)} & \frac{\partial v(t)}{\partial v(t_0)} \end{bmatrix} \tag{15}$$

This transition matrix, $\Phi(t, t_0)$, can be generated by numerically solving the initial value problem:

$$\dot{\Phi}(t, t_0) = \mathbf{A}(t; X_0)\Phi(t, t_0) \tag{16}$$

with;

$$\Phi(t_0, t_0) = I_6 \tag{17}$$

where $\Phi(t_0, t_0)$ denotes that initially all state vectors map over themselves, thus $I_6$ represents a 6-by-6 identity matrix and $\mathbf{A}(t; X_0)$ is the Jacobian matrix of the flow field of the dynamical system evaluated over a reference trajectory (Schaub and Junkins, 2003). The latter can be computed as:

$$\mathbf{A}(t; X_0) = \begin{pmatrix} 0 & -I_3 \\ -G & 2B \end{pmatrix} \tag{18}$$

where;

$$G = -\begin{pmatrix} U_{xx} & U_{xy} & U_{xz} \\ U_{yx} & U_{yy} & U_{yz} \\ U_{zx} & U_{zy} & U_{zz} \end{pmatrix} \tag{19}$$

is the Hessian matrix of the potential function, $U$, Eq.(2), and finally;

$$B = \begin{pmatrix} 0 & 1 & 0 \\ -1 & 0 & 0 \\ 0 & 0 & 0 \end{pmatrix} \tag{20}$$

Hence the transition matrix describing the transformation of an initial state vector to a final state vector with a large time step from $t_0$ to time $t$ can be generated (Koon et al., 2006).

As this method uses the first order equations of motion there will be a loss of accuracy for an increased time step. An error analysis between the method using the transition matrix and the propagation of the equations of motion was performed to determine the maximum length of time for which useable results can be generated. This concluded that for a particle with a displacement of 10,000 km from the equilibrium position, with zero initial velocity, an error in the region of 0.1%, 1% and 10% is achieved for a final time of 56, 155 and 191 days respectively.

An example showing the movement of a 3,000 km radius cloud with a grain $\beta$-value of 0.061 is shown in Fig. 6. It can be seen that the motion of the cloud is away from the $L_1$ point when the initial position is displaced from the equilibrium point. The original cloud becomes stretched with increasing distance from the equilibrium point as the relative dynamics of the particles varies throughout the cloud as described by the state transition matrix, Eq. (15).

## 3. Solar Radiation Model

The solar radiation model (SRM) is used to determine the reduction in insolation due to the presence of the dust cloud. The basic principle of the model is that the path length through the cloud can be found for a line connecting a point on the Sun's surface to a point on the Earth's surface. This path length is then used to calculate the fractional intensity reduction caused by the passage through the cloud.

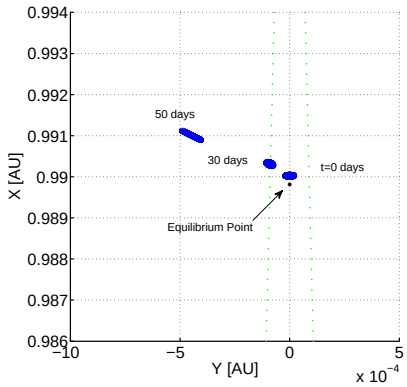


Figure 6: Motion of a 3,000 km radius spherical cloud of particles displaced from the equilibrium position for $\beta = 0.061$ in the $x$-$y$ plane over a period of 50 days. The black dotted lines represent the extent of the useful zone along the Sun-Earth line.

### *3.1. Model structure*

The structure of the SRM can be seen in Fig. 7. The surface of the Earth and Sun will be divided into segments with equal latitude and longitude spacing. At the centre of each segment there will be a node, Fig. 8, which has a surface area and central co-ordinates. The flux contribution to each Earth node provided by each Sun node can be calculated to determine the effect of the dust cloud.

The flux emitted by the Sun node, $I_0$, can be estimated using the following relation;

$$I_0 = I_\odot \Omega A \cos\theta \tag{21}$$

involving the solid angle subtended by an Earth node, $\Omega$, the area of the Earth node, $A$, and the angle of the line-of-sight to the Earth from the surface normal of the Sun, $\theta$, and finally the solar radiance, $I_\odot$, of $2.01 \times 10^7$ W m$^{-2}$ sr$^{-1}$.

The calculation of the solid angle subtended by the Earth node as seen from the Sun node is simplified by assuming that the Earth segment is a flat rather than curved surface but with the same area. The cross-sectional area of the sheet is then found by considering the angle of incidence of the light path in relation to this sheet, which is the angle between the light path and the surface normal, $\phi$. The solid angle is then found by means of Eq. (22), using the distance between the nodes $r$;

$$\Omega = \frac{A\cos\phi}{r^2} \tag{22}$$

Clearly more accurate simulations will use a larger numbers of nodes. This is because as the surface area of each node decreases the assumption of a flat sheet becomes more accurate and also the angle $\theta$ will better represent the whole radiating segment. For the same reason the estimation of the path length through the cloud will be more appropriate for the entire surface segment.

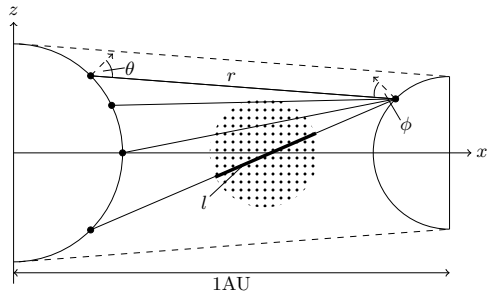


Figure 7: Structure of the SRM where the dashed line shows the extent of the 'useful zone' for insolation reduction.

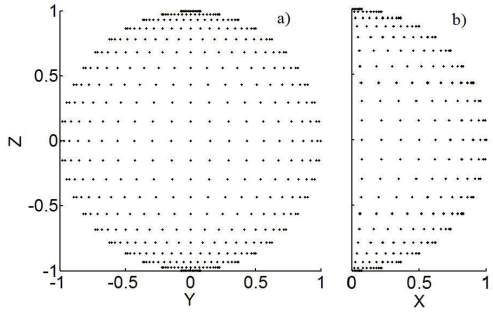


Figure 8: Distribution of 21 × 21 nodes on a spherical surface, as used in the solar radiation model, viewed from the opposite body a) and perpendicular to the Sun-Earth axis b).

### *3.2. Attenuation calculation*

The key to the calculation of the flux received by the Earth node is the use of the Beer-Lambert law for which the general case, Eq. (23), can be seen below;

$$I = I_0 e^{-\int \alpha_{gr}(l)dl} \tag{23}$$

where $I$ and $I_0$ are the intensity of the attenuated and incident light, $l$ is the path-length through the cloud and the factor $\alpha_{gr}$ is the extinction coefficient due to the scattering and absorption of photons. A general approximation of this coefficient is the physical cross-section $\sigma_{gr}$ of the particles multiplied by their number density $\rho_n$. This, in addition to the assumption of homogeneous particle size gives;

$$I = I_0 e^{-\sigma_{gr}\int \rho_n(l)dl} \tag{24}$$

### *3.3. Static model*

A static model was first constructed to test the principles of the SRM. The cloud at $t_0$ is assumed to be spherical with a homogeneous distribution of dust particles with zero velocity. Thus, the particle density in the phase-space can be described as;

$$\rho(\mathbf{x}, \mathbf{v}, 0) = \delta(\mathbf{v}(0)) \cdot H(r_{cloud} - ||\mathbf{x}(0) - \mathbf{x}_{centre}||) \tag{25}$$

where the dirac-delta function $\delta(\mathbf{v}(0))$ describes the initial distribution of the velocity states of the dust as starting from rest, and the Heaviside function $H(r_{cloud} - ||\mathbf{x}(0) -$

$\mathbf{x}_{centre}||$) defines the volume of the spherical cloud of radius $r_{cloud}$ centred at $\mathbf{x}_{centre}$. Here, and for the dynamic model, the path length integral through the cloud, Eq. (24), is calculated by the use of a numerical quadrature method. For the case of the static cloud the density variable is that described by Eq. (25). Thus the solar flux transmitted from each Sun node to each Earth node can be calculated, and hence the flux received by each segment of the Earth's surface can be determined and an intensity map can be constructed.

This cloud model is considered to yield a sufficient accuracy for the initial preliminary analysis intended in this paper, while providing a good compromise on computational effort.

### *3.4. Dynamic model*

For the case of a cloud that has been propagated using the transition matrix, the method involved in calculating the path length is slightly different and can be described as follows:

Assuming that the dynamics of the dust cloud satisfies Liouville's Theorem, which is equivalent to neglecting dissipation of energy by processes such as inelastic collisions, fragmentation or coalescence, one can define the density on the phase space at time t as:

$$\rho_\Gamma(\mathbf{x}, \mathbf{v}; t) = \rho_\Gamma(\phi^{-t}(\mathbf{x}, \mathbf{v}); 0) \tag{26}$$

where $\phi^{-t}(\mathbf{x}, \mathbf{v})$ denotes the flux of the system, or evolution of the state $X(t) = [\mathbf{x}(t)\ \mathbf{v}(t)]^T$ over a time-span $-t$ so that $\phi^{-t}(\mathbf{x}, \mathbf{v})$ is equal to $[\mathbf{x}(-t)\ \mathbf{v}(-t)]^T$. This *flux* of the system can be computed as described by Eq. (14), which requires the transition matrix, as seen in Eq.(15), to be computed. Now, since the density of dust particles for a given time $t$ is required, the phase space density, $\rho(\mathbf{x}, \mathbf{v}; t)$, must to be integrated over the velocity components at time $t$:

$$\begin{aligned}\rho(\mathbf{x}; t) &= \int_\Gamma \rho_\Gamma(\mathbf{x}, \mathbf{v}; t) d\upsilon(t) \\ &= \int_\Gamma \rho_\Gamma(\phi^{-t}(\mathbf{x}, \mathbf{v}); 0) d\upsilon(t)\end{aligned} \tag{27}$$

where $d\upsilon(t)$ is the product of the one-dimensional differential components of the velocity, $dv_x \cdot dv_y \cdot dv_z$. Now, Eq.(27) can be rewritten using Eq.(25) as:

$$\rho(\mathbf{x}; t) = \int_\Gamma \delta(\phi^{-t}(\mathbf{x}, \mathbf{v})_\mathbf{v}) \cdot H(r_{cloud} - ||\phi^{-t}(\mathbf{x}, \mathbf{v})_r||) d\upsilon(t) \tag{28}$$

where $\phi^{-t}(\mathbf{x}, \mathbf{v})_r$ and $\phi^{-t}(\mathbf{x}, \mathbf{v})_\mathbf{v}$ are, respectively, the components of the position and velocity of the *flux*, $\phi^{-t}(\mathbf{x}, \mathbf{v})$. The integral in Eq. (28) can be solved using the Dirac delta definition by substituting the infinitesimal volume of the phase space $d\upsilon(t)$ by:

$$d\upsilon(t) = \left\| \frac{\partial \mathbf{v}(t)}{\partial \mathbf{v}(0)} \right\| d\upsilon(0) \tag{29}$$

Thus resulting in;

$$\rho(\mathbf{x}; t) = \left\| \frac{\partial \mathbf{v}(t)}{\partial \mathbf{v}(0)} \right\| H(r_{cloud} - ||\phi^{-t}(\mathbf{x}, \mathbf{v}_*)_r||) \tag{30}$$

where $\mathbf{v}_*$ is the solution of the equation $\phi^{-t}(\mathbf{x}, \mathbf{v}_*)_v = 0$, such that $\delta(\phi^{-t}(\mathbf{x}, \mathbf{v})_v) = 1$.

This definition of the density can then be substituted into Eq. (24) to enable the solar insolation reduction to be found for any time.

### *3.5. Static model testing*

To test the accuracy of the SRM, the average solar insolation over the Earth's surface can be found for different numbers of longitude and latitude nodes on the Sun's surface whilst the number of nodes on the Earth's surface remained constant at $21 \times 21$. The results can be seen in Fig. 9. This shows that as the number of nodes increases the solar constant levels off quickly to a value of 1381.9 W m$^{-2}$. This value compares favourably against those found in the literature e.g. 1367 W m$^{-2}$ (Govindasamy et al., 2003) or 1371 W m$^{-2}$ (de Pater and Lissauer, 2001) as there is an approximately 1% difference at the highest number of nodes used.

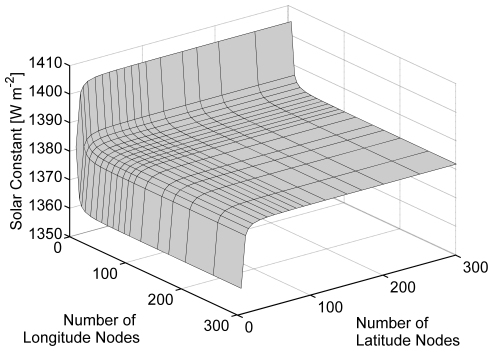


Figure 9: Average solar constant over the Earth's surface obtained using the SRM for varying numbers of longitude and latitude nodes on the surface of the Sun.

A similar test was carried out to determine the number of longitude and latitude nodes required on both surfaces to provide a reliable result of the insolation change. This test essentially aims to determine the node number where a further increase would lead to a negligible change in the result. This was performed by placing a spherical cloud of radius 4,000 km with a grain size of 10 $\mu$m and number density of 110 m$^{-3}$ at the $L_1$ position. The average solar constant on the Earth's surface was then calculated for varying numbers of nodes on the surfaces of both bodies with the number of longitude and latitude nodes being equal. The *quadgk* function in MATLAB, using adaptive Gauss-Kronrod quadrature, is used for this process. The result of this test can be seen in Fig. 10. This shows a similar shape to that seen in Fig. 9 and it can be concluded that node numbers of $61 \times 61$ is the number required to

produce a consistent result. The variation in the result between this number of nodes and the highest used, $151 \times 151$ nodes, is of the order $10^{-5}$. However, it is possible to use $21 \times 21$ nodes on the surfaces of both bodies with a variation from the highest node result of the order of $10^{-4}$. The motivation for finding the minimum number of nodes is to minimise the computation costs. For example, a simulation involving $41 \times 41$ nodes on each sphere requires 15 times more path length calculations in comparison to a $21 \times 21$ simulation. Thus using $21 \times 21$ nodes rather than $61 \times 61$ nodes will considerably decrease the computational requirement whilst maintaining an acceptable level of accuracy. As an example, to calculate a data point shown in Fig. 13 or Fig. 14 for $21 \times 21$ nodes took 2.1hr to calculate whilst the same point for $61 \times 61$ nodes took 143.5hr for a 3GHz processor.

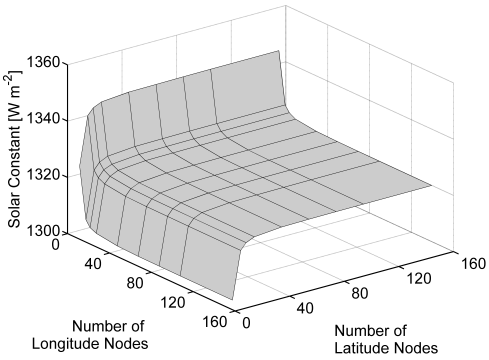


Figure 10: Average solar constant on the Earth's surface calculated for varying node numbers in a test of the SRM using a 4,000 km cloud placed the L1 point.

## 4. Results

### *4.1. Stability analysis*

The stability analysis begins by considering the simplest case, a spherical cloud of dust of uniform density with a grain $\beta$-value of zero placed at the classical $L_1$ point. For all cases considered the initial velocity is assumed to be zero. For various radii of cloud the movement of a sample of evenly spaced test particles can be observed using the transition matrix, Eq. (14). The lifetime of a particle is then determined to be the length of time that it is in a position to block solar photons near the Sun-Earth line. The boundary of this 'useful zone' can be seen in Fig. 6 and Fig. 7. For cloud radii from 500-14,000 km the average lifetime of these test particles can be seen in Fig. 11. The maximum size of 14,000 km was chosen as this is the approximate extent of the useful zone at the classical $L_1$ point. It can clearly be seen that the average lifetime of the particles decreases significantly with cloud radius. This result sets a limit for later stability analyses as the effect of SRP is not added. It is expected, therefore, that for the scale of dust grains investigated, the average lifetime of the dust particles will fall below this level when the cloud remains at the $L_1$ point. In contrast it is expected that the average lifetime of a cloud placed at the displaced equilibrium position should increase slightly with $\beta$ due to the reduced gradient of the potential function at this position.

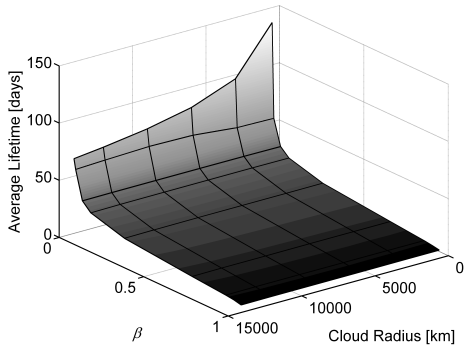


Figure 11: Average lifetime of particles in a dust cloud positioned at the classical $L_1$ point for varying radii and values of $\beta$.

The average lifetime of a cloud positioned at the $L_1$ point for varying radii and $\beta$-values can also be seen in Fig. 11. This shows that when SRP is taken into account the average lifetime of particles within the cloud decreases significantly when placed at the classical $L_1$ point, as expected. This is irrespective of cloud radius, though the smaller clouds do show a slightly increased average lifetime. As noted previously, this is due to the increased displacement from the classical equilibrium point. In contrast, when a cloud is centred at the new displaced equilibrium point the average lifetime increases with $\beta$, Fig. 12. Again the smaller cloud radii have longer lifetimes. This increased lifetime is due to the shallower gradient of the potential function caused by the decrease in the effect of solar gravity as $\beta$ increases. Comparing these results indicates that a cloud placed at the displaced equilibrium point is likely to be a more mass efficient option. However, it cannot yet be concluded that this equilibrium point is the most suitable position without taking into account the engineering challenges involved.

### *4.2. Dynamic solar radiation model results*

The key quantifiable parameter for this method of geoengineering is the cloud mass necessary to create the required level of solar insolation reduction. This shall be presented in terms of the mass per year of asteroid material required. This is calculated using the SRM as described in Sec. 3.4 which allows the path length through the cloud to be calculated for any given time. Hence, the evolution of the reduction in solar insolation due to the cloud dynamics can be found for different initial cloud and grain radii.

The results shall be found for dust clouds placed at the classical Lagrange point and the new displaced equilibrium points created for different $\beta$-values of asteroidal material.

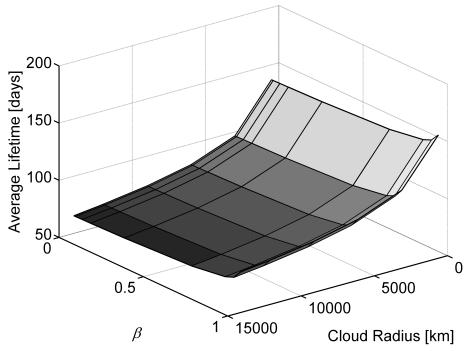


Figure 12: Average lifetime of particles in a dust cloud positioned at the displaced equilibrium point for varying radii and values of $\beta$.

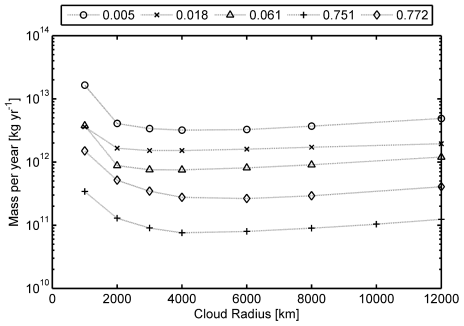


Figure 13: Mass requirement of dust for the steady state solution of clouds ejected at the $L_1$ point for varying initial cloud radii for the five grain $\beta$-values used.

The initial clouds are assumed spherical with sizes ranging from 1,000-12,000 km for five different grain sizes. These grain dimensions are based on the investigation performed in (Wilck and Mann, 1996) and are radii of 32, 10, 3.2, 0.32 and 0.1 $\mu$m which correspond to $\beta$-values of 0.05, 0.018, 0.061, 0.772 and 0.751 respectively as seen in Fig. 4. In terms of terrestrial aerosol particles the three larger grain sizes correspond to relatively coarse particles e.g. terrestrial silt particles blown up by the wind. In contrast the smaller particles correspond to the size of condensed gas particles. The equilibrium points for the different particles are displaced sunwards of the conventional $L_1$ point by 950,000 km, 875,000 km, 32,000 km, 9,000 km and 2,500 km for the $\beta$-values used from 0.772 to 0.005 respectively.

Each result was calculated using 20 time steps with the length of each step being dependent upon the lifetime of the cloud. A steady state solution is then calculated using the combined effect of the cloud at each time step by summing the relative phase-space densities, as in Eq. (30), for the times used for each individual path.

$$I = I_0 e^{-\sigma_{gr} \int_{t_0}^{t} \int \rho(l,t) dl dt} \tag{31}$$

$$= I_0 e^{-\sigma_{gr} \sum_{t_n=0}^{20} \int \rho(l,t_n) dl} \tag{32}$$

Following this, the initial density of the cloud was optimised to achieve the required 1.7% insolation reduction when the attenuation is calculated. Subsequently, knowing the time step and grain properties, the mass that is required to be ejected per year can be determined. The results for all five grain sizes for clouds ejected at the $L_1$ point can be seen in Fig. 13.

In general the result expected was that the larger particles, which have smaller values of $\beta$, would require less mass per year due to their greater average lifetime. This is not the case however and it appears that the decrease in grain size provides a greater mass saving than the longer lifetime of the larger particles with the optimum solution occurring for the smallest grain radius of 0.1 $\mu$m.

For the optimum cloud radius of 4,000 km, which is similar to the stationary SRM result, the mass requirement is $7.60 \times 10^{10}\,\mathrm{kg\,yr^{-1}}$. In comparison to the method proposed by Struck this is a mass saving of several orders of magnitude. For this scenario the average mass ejection rate must be of the order of $850\,\mathrm{kg\,s^{-1}}$. The feasibility of this estimate will be discussed later. The results for the steady state solution for a cloud ejected at the equilibrium point can be seen in Fig. 14. It shows a similar shape to the results shown in Fig. 13 with the optimum mass requirement being $2.93 \times 10^{9}\,\mathrm{kg\,yr^{-1}}$.

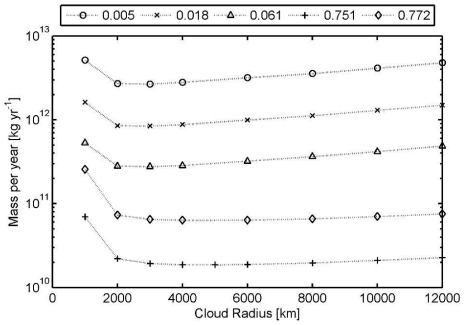


Figure 14: Mass requirement of dust for the steady state solution of clouds ejected at the new displaced equilibrium points of the four grain $\beta$-values used for varying initial cloud sizes.

The result for the case of a 0.1 $\mu$m grain is clearly more optimal than for larger grains in more than just the mass requirement. Although this is partly a product of the method used to generate the steady state solution, the shorter lifetime of the smaller radius particles requires the insolation change to be achieved in a shorter time than for the larger particles. Fig. 15 shows the time to achieve a steady-state for grain radii of 3.2 $\mu$m, this value is shown rather than for 0.1 $\mu$m for clarity, and 32 $\mu$m where at each time step a new cloud is released. As can be seen, the 3.2 $\mu$m case reaches the desired insolation change in approximately 20-30 days whilst the 32 $\mu$m case takes of the order of 100 days. For a grain size of 0.1 $\mu$m this falls to approximately 10 days.

The same principle applies to the deactivation period for the cloud. When geoengineering is no longer required,

or if the cloud proves to have unforeseen side-effects on the Earth's climate and must be discontinued, then the lower grain size cloud will be beneficial since the cloud will disperse in a much shorter time. This will not apply to a scheme where the cloud is released at the classical equilibrium point however, as the smaller particles are likely to have a longer lifetime.

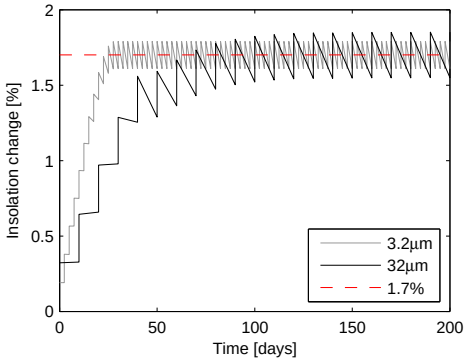


Figure 15: Variation in insolation change expected during the activation phase of the geoengineering method for the case of a cloud of 32 $\mu$m and 3.2 $\mu$m sized grains placed at the $L_1$ point for a final insolation change of 1.7%.

The change in insolation seen in Fig. 15 appears highly uneven. This is due to the periodic mass ejections used to generate the steady state condition. A steady state condition based on a continuous ejection of mass would eliminate this 'flickering' effect.

A map showing the insolation change over the Earth's surface for a cloud of radius 4,000 km and grain size 0.1 $\mu$m released at the $L_1$ point and the new displaced equilibrium point for $61 \times 61$ nodes on the surface of each body can be seen in Fig. 16 and Fig. 17. It should be noted that the tilt of the Earth's axis is not taken into account. As can be seen, the schemes where the cloud is released at the new displaced equilibrium point show a more symmetrical pattern. The insolation appears evenly spread as the cloud is initially positioned directly along the Sun-Earth line. This is additionally caused by the largest dispersion of the cloud occurring within the ecliptic plane whilst dispersion does not occur along the z-axis. The insolation change map for the case of a cloud released at the classical $L_1$ point shows a different pattern. Here the insolation change is shifted towards one side of the Earth due to the movement of the cloud away from the initial position being in one direction. This will lead to greater shading in the 'morning' region of the Earth. The effects of this are not yet known, but an attempt to quantify this will be an interesting avenue of future research.

### *4.3. Anticipated accuracy*

A final issue concerning the accuracy of the methodology proposed here can be tackle by comparing the particle evolution by using both the transition matrix and direct

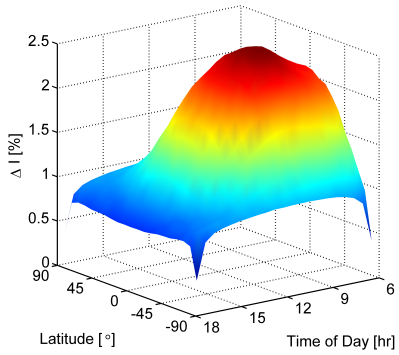


Figure 16: Percentage insolation change over the surface of the Earth for the steady state solution of an initial cloud of radius 4,000 km and grain size of 0.1 $\mu$m released at the classical $L_1$ point.

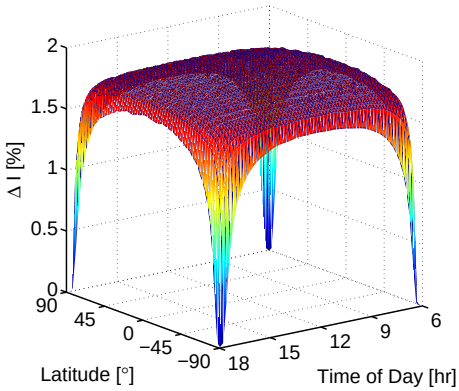


Figure 17: Percentage insolation change over the surface of the Earth for the steady state solution of an initial cloud of radius 4,000 km and grain size of 0.01 $\mu$m released at the displaced equilibrium point.

propagation of the equations of motion, Eq. (1). The results show that high $\beta$-value clouds are relatively highly affected by propagation error, accumulating averages of 10% error after only a few tens of days. Fortunately, on the steady state solution the dust that has been drifting for these periods only contributes less than 5% of the solar insolation reduction, thus the overall accuracy of the method is not compromised.

## 5. Discussion

From section 4 the mass of asteroidal material required to create an insolation change of 1.7% for dust clouds placed at the classical Lagrange point and new displaced equilibrium point has been calculated to be $7.60 \times 10^{10}\,\mathrm{kg\,yr^{-1}}$ and $1.87 \times 10^{10}\,\mathrm{kg\,yr^{-1}}$ respectively. This is considerably lower than the dust cloud methods suggested in (Struck, 2007) and (Pearson et al., 2006). It is also in line with the solid reflector/refractor proposals in (Angel, 2006) and (McInnes, 2010) whilst reducing the need for manufacturing considerably. As well as mass, the first order feasibility of these different methods can

be compared using the energy required to be placed in the required position. This shall be discussed in the following section before the engineering requirements of the different cloud generation mechanisms will be discussed to determine the feasibility of this method.

### *5.1. Comparison to previous proposals*

The estimates of the energy required for each of the discussed proposals can be seen in Table 1. The energy required to launch a 2,100 kg spacecraft, with 1,000 kg payload, to the $L_1$ point using a mass driver is estimated by Angel to be $6.35\times10^{11}$ J (Angel, 2006). This results in a total energy requirement of $1.27 \times 10^{19}$ J. It can be assumed that the solid reflectors proposed by McInnes can be launched in a similar fashion, thus giving an energy requirement of $1.78 \times 10^{20}$ J.

Struck comments on the capture of comets or use of lunar material as possible sources for the dust cloud. A lower bound on the energy required for the proposal by Struck can be made by computing the change in Jacobi constant associated with moving material from a worst case of the Sun-Earth $L_4/L_5$ points to the equivalent points in the Earth-Moon system. This provides an estimate of $2.2 \times 10^{20}$ J. Alternatively, the energy required to overcome the gravitational potential associated with moving an object from the surface of the Moon to the Earth-Moon $L_4/L_5$ points can be determined. This gives an energy of $5.9\times10^{20}$ J though in reality a greater mass will be needed to account for the spacecraft that are required to deliver the lunar dust. By following the methods used by Angel for a mass driver but neglecting losses due to atmospheric drag and the associated shielding gives an energy of $4.6 \times 10^{21}$ J.

The energy requirement for the two proposals made by Pearson for a dust ring and satellite ring can similarly be estimated using the methods described by Angel. These energies are $2.0\times10^{18}$ J and $2.4\times10^{18}-1.0\times10^{21}$ J for the satellite ring and dust ring respectively. These energies are optimistic in the respect that the atmospheric drag is likely to be greater than calculated. This is because to achieve the orbital radius required of 1.2-1.6 times the radius of the Earth the elevation of the mass driver tube will be much lower than for a journey to $L_1$. In comparison, for the dust ring, the energy required to capture the material in the form of a near Earth object is $8.9 \times 10^{19}$ J. This was calculated in a similar way to for the estimate for the Earth-Moon system dust cloud. An additional factor must be added to the energy of the particle ring. This is the energy required to capture two shepherding asteroids, the upper mass of which is $1.4 \times 10^{11}$ kg. This will add an extra $5.4 \times 10^{18}$ J to the dust ring energy.

A similar estimate can be used to determine the energy required to manoeuvre the necessary mass of asteroid material to the $L_1$ position for the method proposed in this paper. Assuming that geoengineering is required for a minimum duration of 10 years the energy required to capture the required material is approximately $1.5 \times 10^{17}$ J. This figure will be increased when the energy required to launch the spacecraft used to capture the NEA is taken into account but this can be assumed to be negligible in comparison to the mass of the asteroids. The method of geoengineering proposed in this paper can be seen to have a lower energy requirement than other proposals. As a comparison, the energy required for this proposal is equivalent to the maximum generation capacity of the Three-Gorges Dam running continually for approximately 3 months. Using the same comparison, the mass of concrete used to construct the Three-Gorges Dam is in the region of $10^{10}$ kg. Hence the geoengineering schemes discussed here will be large ventures, highlighting why the engineering demands of space-based geoengineering must be reduced.

### *5.2. Material availability*

The optimum mass requirements calculated for a cloud released at the classical $L_1$ and new equilibrium points are both significant. Nevertheless, these results represent orders of magnitude improvement with respect to previous concepts envisaging the passive use of dust as a geoengineering method (Pearson et al., 2006; Struck, 2007). A paramount issue for any geoengineering proposal requiring dust or raw material is the source of this material and its accessibility.

By assuming here that the accessibility of asteroid/comet material from the Sun-Earth $L_1$ is, as a first approximation, similar to the asteroid accessibility from weakly-bound Earth orbits, the approximated amount of material accessible at an energy lower than that required to exploit the Moon can be shown to be of order $6\times10^{13}$kg (Sanchez and McInnes, 2011). This estimation results from summing up the mass of all objects, described by a Near-Earth object population distribution, that can reach a weakly-bound Earth orbit (i.e., Earth parabolic orbit) with a total $\Delta v$ budged lower than $2.37\,\mathrm{km\,s^{-1}}$ (i.e., Moon's escape velocity) (Sanchez and McInnes, 2010, 2011). In particular, for the value presented here a three impulse transfer model was used to assess the $\Delta v$ cost of the transfer (Sanchez and McInnes, 2011). Thus, this result suggests that the geoengineering scheme proposed, Sun-Earth $L_1$ dust cloud, could be theoretically sustained for 3,000 years by depleting all the asteroid/comet material that is energetically more accessible than the surface of the Moon (and therefore also the Earth and anywhere else in the Solar System). On the other hand, Struck's Earth-Moon $L_4/L_5$ dust cloud could not be generated even by depleting the same asteroid material. Moreover, in order to provide asteroid material for a planetary dust ring in low Earth orbit, as suggested by Pearson (Pearson et al., 2006), would require an extra $3.3\,\mathrm{km\,s^{-1}}$ to transport this material to the required position.

Furthermore, Sanchez and McInnes (Sanchez and McInnes, 2010) describe how to estimate the $\Delta v$ cost to access individual objects as a function of object size. A simplified version of Fig. 10 in (Sanchez and McInnes, 2010) is presented here as Fig. 18. This figure shows

the average available resources by using the first, tenth, hundredth and thousandth largest accessible asteroid or cometary object in near Earth space. The figure also represents the 90% confidence region, which accounts for the statistical uncertainty of the Near-Earth object population distribution. This particular figure has been updated with the accessibility provided by the three impulse transfer model as described in (Sanchez and McInnes, 2011).

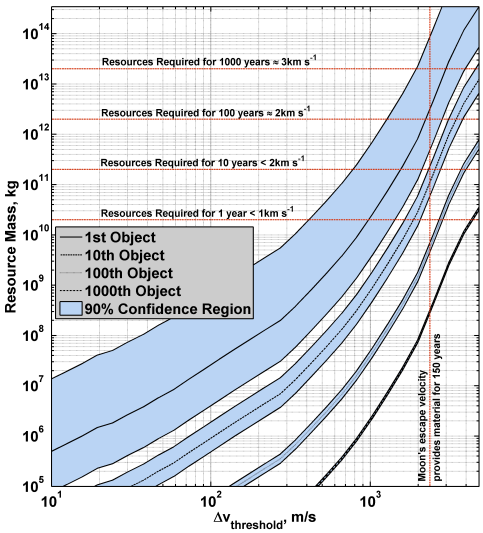


Figure 18: Expected resources for each statistical accessible object.

Figure 18 suggests that it is possible to find objects able to sustain the $L_1$ dust cloud concept for at least 150 years with a $\Delta v$ lower than that required to exploit the Moon. The minimum size object to sustain the cloud for 1 year is found to be accessible with a $\Delta v$ of order $1\,\mathrm{km\,s^{-1}}$, while $3\,\mathrm{km\,s^{-1}}$ would be needed to provide 1 large object able to sustain the concept for 1,000 years. This, of course, assumes that all the material on the asteroid is milled to fine dust and expelled. These are general feasibility considerations on the availability of the material, which strongly suggests the benefits of using dust sourced in-situ over previous published dust-cloud concepts.

### *5.3. Cloud generation*

The feasibility and challenges associated with manufacturing the dust cloud using solar concentrators, mass driver equipped landers and by spin fragmentation will now be discussed. This shall focus on their ability to manufacture the desired grain sizes and the probable deployment state with some brief comments on other engineering aspects.

#### *5.3.1. Solar collector/sublimation*

The sublimation method involves heating the surface of an asteroid to high temperatures such that material sublimates directly from a solid to a gas. This technique has been investigated for asteroid hazard mitigation and is a novel approach that can either be performed with a laser or a large solar collector. The latter method was first proposed in (Melosh et al., 1994) and will be the method discussed here. The results for the two methods will in principle be similar, due to the adiabatic expansion involved with both the solar collector and laser ablation methods Kahle et al. (2006); Anisimov et al. (1996).

An analysis of the physical principles and practical implications of this method was examined in (Kahle et al., 2006). It was concluded that the plume of material created is analogous to the expansion of a gas exiting a nozzle into a vacuum. The mass flux, $Z$, leaving the asteroid and the average velocity, $v$, of the particles can be estimated using the relationships in Eq. (33) and Eq. (34) respectively;

$$Z = \frac{p_{spot}}{\sqrt{2\pi R_s T_{spot}}} \tag{33}$$

$$v = \sqrt{\kappa R_s T_{spot}} M_n \left(1 + \frac{\kappa - 1}{2} M_n^2\right)^{-1/2} \tag{34}$$

For an S-class asteroid, comprised mostly of silicate based minerals, it is acceptable to assume that it is comprised solely of forsterite. It follows that the specific gas constant, $R_s$, for diatomic forsterite has a value of $206.7\,\mathrm{J\,kg^{-1}K^{-1}}$ and that the gas pressure at the beam spot, $p_{spot}$, can be calculated as follows;

$$p_{spot} = C_1 e^{C_2/T_{spot}} \tag{35}$$

Here the constants $C_1$ and $C_2$ have the values $7.62 \times 10^{13}$ Pa and -65,301 K respectively. The spot temperature, $T_{spot}$, was shown by Kahle to increase with the illumination time of the spot before reaching a value in the region of 2280 K.

Kahle concluded that for a solar collector with a diameter of 630 m creating a spot of diameter 16 m the mass flux is $16\,\mathrm{g\,m^{-2}\,s^{-1}}$. The result is a mass flow rate of $3.2\,\mathrm{kg\,s^{-1}}$. This means that for the mass ejection rate requirements of the clouds ejected at the classical $L_1$ and new displaced equilibrium points to be met 200-300 solar collectors would be required. This is a significant requirement. However, this remains considerably lower than the quantity of solar reflectors required to create the total insolation change in conventional approaches to geoengineering.

The velocity of the ejected plume can be estimated to be $741\,\mathrm{m\,s^{-1}}$ at the throat when the heat capacity ratio, $\kappa$, is 1.4 and the Mach number, $M_n$, at the throat is 1. After this the gas will expand, increasing in speed until the transition boundary between the continuum and free-molecular flow is reached. After this point the velocity is constant. By following the principles described in Kahle, the velocity at this point can be found to be $1.79\,\mathrm{km\,s^{-1}}$. This velocity is too high for the assumptions of the static cloud in this paper to hold and therefore further studies must be performed on clouds with an initial velocity.

The ejected gas particles will be approximately 0.2 nm in diameter. As such they will be considerably smaller than the scale used in this paper. However, the gas particles will likely re-condense to form larger particles, once

ejected, and furthermore, it can be assumed that larger particles will also be emitted from the spot as some grains will be ejected by the flow of gas before being completely sublimated. Such larger particles will likely have lower velocities than the gas plume due to the equipartition of energy. The scale of these effects cannot yet be determined though they may increase the feasibility of this method due to the greater mass efficiency.

The final consideration for this method is the complexity and reliability of the systems involved. Firstly, it will be complex to provide an autonomous control system for the several hundred collectors required. Secondly, the lifetime of the collectors may be short, a matter of hours, due to the impingement of the ejected dust on the surface of the collectors Kahle et al. (2006). It is noted that the lifetime can be increased greatly by the use of a smaller secondary mirrors to re-focus the collected sunlight to reduce contamination. Several of these secondary mirrors can be used and rotated once contaminated to increase the lifetime.

*5.3.2. Mass driver*

A mass driver concept would involve a spacecraft landing on the surface of a suitably large asteroid and then extracting material from the surface. This material would then be ejected using the mass driver. The extraction technique would be required to generate the correct, or similar, scale of dust material and therefore some processing will likely be required.

Mass drivers are generally envisaged as high velocity devices, most suitable for launching objects into orbit cheaply and efficiently. However, they could also be used for low ejection velocity applications. An advantage of this method is that the ejection velocity can be more greatly controlled than for the solar collector method.

The use of mass drivers for asteroid hazard mitigation has previously been investigated for a spacecraft design that incorporates a nuclear reactor powered mass driver (Olds et al., 2004). A swarm of these 500-1000 kg spacecraft are envisaged landing on an asteroid and ejecting material from the surface with a velocity of $187\,\mathrm{m\,s^{-1}}$ at the rate of approximately $120\,\mathrm{kg\,hr^{-1}}$. As with the case of the solar collector spacecraft, many of these units would be required to meet the ejection rate demands, in the region of several thousand. However these vehicles have been designed to maximise the impulse generated on the host asteroid and hence may not be best suited for the scenario envisaged in this paper. In addition, as with the case of the solar collector the velocity of the ejecta may not be optimum for this scenario and therefore it can be imagined that, assuming the same spacecraft power consumption, a greater mass of material could be launched at lower velocities.

The complexity of this scenario is not as great as for the solar collector concept as there is no complex motion of the spacecraft. Some control is required to ensure that the required thrust is in the correct direction to maintain stability of the asteroid at $L_1$ or in its orbit (discussed later) however this will be small in comparison. The key issue in this case is the lifetime of the mining equipment. As there is significant of terrestrial heritage, the average lifetimes of the excavating and processing equipment is likely to be at least several years.

*5.3.3. Spin fragmentation*

An additional method of cloud generation is the possibility of imparting angular momentum to an asteroid such that the rotation rate increases. It is considered that a large number of small asteroids are 'rubble piles' (Harris, 1996) loosely held together by self-gravity, and as such material could easily be ejected from the surface under the correct conditions.

The angular velocity required, $\omega_{crit}$, to cause the liberation of material can be estimated by equating the centripetal and gravitational forces. This relationship, can be found to depend only on the mass, $M_a$, and radius, $R_a$, of the asteroid and is;

$$\omega_{crit} = \sqrt{\frac{GM_a}{R_a^3}} \tag{36}$$

This would be sufficient to eject the regolith from the surface of the asteroid, however a larger angular velocity would be required to tear apart the asteroid. It has been suggested that a sub-kilometre sized asteroid can be spun-up to the point of fragmentation by the use of tethered satellites transferring torque in the same manner as a reaction wheel (Bombardelli, 2009). The scale of material ejected in this scenario is likely to vary greatly as it will depend on the grain size of the surface of the asteroid as well as the internal structure. It is unlikely that the material could be ejected at the displaced equilibrium point and hence this method of cloud generation is best suited for creating clouds at the $L_1$ point. An additional factor that must be considered is that the cloud shape obtained from spinning an asteroid is likely to be a disk rather than a sphere. Further research into the stability and attenuation properties of a disk shaped cloud must be researched to fully determine the feasibility of this cloud generation method. Finally, the engineering challenge of this method is considerable as the tether length required to spin-up a reasonably sized asteroid is in the region of several kilometers but also the method to transfer the torque to the asteroid will be complex.

*5.3.4. Summary*

None of the generation methods discussed fulfill all the requirements for the static cloud scenario. The solar collector method is very complex whilst enabling little control over the size and velocity of the ejected particles. Furthermore, the lifetime of the solar collectors is likely to be short requiring large numbers to be manufactured for this purpose, in part negating the benefits of the dust cloud

method. The spin fragmentation method is also not suitable as there is little control over the sizes of the ejected grains though the overall complexity is lower as far fewer spacecraft will be required. However, significant challenges remain in transfering the torque to the asteroid. The mass driver is the most suitable of these methods as there is the greatest level of control over the system. Before it can be concluded that it is suitable the effects of the initial velocity on the spread of the cloud should be determined. The methods are rated in terms of complexity, reliability, cloud characteristics and efficiency in Table 2 based on the factors discussed previously.

### *5.4. Comparison to solar reflector manufacture in-situ*

An interesting comparison for the proposed geoengineering scheme is with manufacturing solar reflectors in-situ using captured asteroid material. At a qualitative level this may be a viable scheme, given the appropriate technology becomes available, and it may have some significant advantages over terrestrial based manufacture and launch. As well as the key advantage that the reflectors will not need to be launched to $L_1$, the conditions for manufacturing may be superior in space. As suggested in (Lippman, 1972) the main limitations on the thinness of manufacturing films are gravity, electrostatics and contamination. An additional factor is the oxidisation of the film which will change the reflective properties of the surface and hence the perturbation by SRP. As such solar reflectors manufactured in the vacuum of space are likely to be of higher quality than terrestrial manufacture. The disadvantage in this method however is that the manufacture process will need to be automated which will increase the level of complexity greatly. Lippman used the example of a heliogyro film to analyse the feasibility of such manufacturing techniques in laboratory experiments. A deposition rate of $0.2\,\mathrm{kg\,hr^{-1}}$, corresponding to an area of $27.8\,\mathrm{m^2\,hr^{-1}}$, was found to be achievable though no comment was made on higher deposition rates.

There is some further precedent to automated manufacture, for example recently commercialised 3D printers. Given future technological development it may be possible to 'print' solar reflectors in-situ given the correct bulk material is available. This again leads to the possibility of capturing asteroids from which material can be extracted and used in manufacture. For example an M-class asteroid is mostly comprised of iron and nickel elements which could be used in the fabrication of reflectors. Additionally, S-class asteroids are mostly comprised on silicate based minerals such as forsterite which also contain large amounts of magnesium which would also be a suitable material for reflector manufacture.

A model can be constructed to estimate the time scale required to manufacture the required area of solar reflectors, as suggested by McInnes to be of order $6.57\times10^6\,\mathrm{km^2}$ (McInnes, 2010), given several different scenarios. The first scenario will estimate the time taken to eject the required mass of material from an asteroid, using the plume model suggested in (Kahle et al., 2006), given an initial solar collector diameter of 630 m, while assuming there is no time lag required to manufacture subsequent reflectors. The second scenario will estimate the time required for manufacture by selecting the longest time from either the time to gather the material or the time to deposit based on different deposition rates. The results can be seen in Fig. 19.

This clearly shows that the manufacturing rate is the major limiting factor with the highest value of $1\times10^6\,\mathrm{kg\,hr^{-1}}$ requiring in the region of 30 years to produce the necessary area of solar reflector. Should the technology become feasible, there are advantages to this approach as the time required for manufacture enables observations of changes in the Earth's climate to be made before fully committing to the scheme.

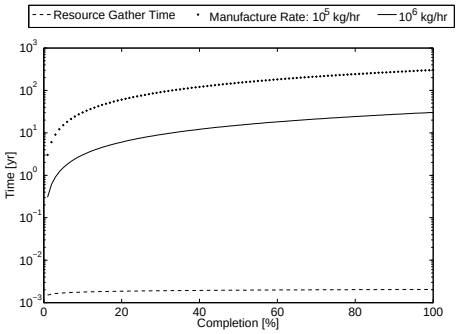


Figure 19: Manufacturing times for the required area of thin film solar reflectors suggested in (McInnes, 2010) for different mass deposition rates for in-situ fabrication.

### *5.5. Asteroid positioning*

It is desired that the asteroid is placed at the centre of the cloud, either the $L_1$ or neighbouring equilibrium positions, to enable continual ejection of material. Therefore, a key technological requirement is the ability to stabilise an asteroid at or near $L_1$. This is likely to be possible for the $L_1$ position using the mass ejection methods discussed previously e.g. the solar collector or the mass driver, providing the velocity when approaching $L_1$ is small enough. As already stated these methods are most commonly investigated with the aim of providing an impulse to an asteroid for hazard mitigation purposes and hence this is not unfeasible. The requirement to have multiple mass ejectors to achieve the mass ejection rate requirements will prove to be an advantage in terms of the control available over the asteroid. Using multiple thrust vectors will enable a more precise stabilisation to be achieved. It should be noted that thin film reflectors deployed near $L_1$ will also require active stabilisation of a system with a significant mass.

For the case of the equilibrium position it will not be possible to completely stabilise the asteroid as the equilibrium is only for a given $\beta$ value. Instead, the likely scenario would involve placing an asteroid on a periodic orbit

around $L_1$, such as a Lyapunov orbit with the maximum displacement along the Sun-line passing through the equilibrium position. Material would then be ejected within a region closest to this position. To reduce the requirements on the mass ejection system, several asteroids would be required, regularly spaced along the same orbit.

A factor that must be considered is the risk presented to Earth due to the presence of the asteroids used to generate the cloud. To capture a single asteroid to supply the dust cloud for many years would clearly be a threat to the Earth. However, it is possible to capture a greater number of smaller asteroids, or at the very least, break off chunks of larger rubble pile asteroids in a close approach to Earth. These would individually not pose a significant threat.

## 6. Conclusion

In this paper a method of geoengineering has been proposed involving clouds of dust placed in the vicinity of the $L_1$ point as an alternative to the use of thin film reflectors. It has been concluded that the mass requirement for a cloud placed at the classical $L_1$ point, to create an average solar insolation reduction of 1.7%, is $7.60 \times 10^{10}\,\mathrm{kg\,yr^{-1}}$ whilst a cloud placed at a displaced equilibrium point created by the effect of solar radiation pressure is $1.87 \times 10^{10}\,\mathrm{kg\,yr^{-1}}$. These mass ejection rates are considerably less than the mass required in the methods proposed in (Struck, 2007) and (Pearson et al., 2006) and are comparable to the thin film reflector methods proposed in (Angel, 2006), (McInnes, 2010) and others. It has also been shown that the energy required to position the method proposed here at the $L_1$ position is less than other methods. In addition, it has been shown that the mass required to sustain this proposed geoengineering method for at least 150 years can be captured from the near-Earth object population for a maximum $\Delta v$ that is lower than that required to exploit the Moon, $2.37\,\mathrm{km\,s^{-1}}$. It is envisaged that, once a near-Earth object has been captured, it can be stabilised in the required position using the impulse provided by solar collectors or mass drivers used to eject material from the surface.

## 7. Acknowledgements

The work reported in this paper was funded by the European Research Council through VISIONSPACE (project 227571).

## 8. References

## References

Angel, R., Feasibility of cooling the Earth with a cloud of small spacecraft near the inner Lagrange point (L1), Proceedings of the National Academy of Sciences, 103, 17184-17189, 2006.

Anisimov, S. I., Luk'yanchuk, B. S. and Luches, A., An analytical model for three-dimensional laser plume expansion into vacuum in hydrodynamic regime, Applied Surface Science, 96-98, 24-32, 1996.

Binzel, R.P., Rivkin, A.S., Thomas, C.A., et al., Spectral properties and composition of potentially hazardous Asteroid (99942) Apophis, Icarus, 200, 480-485, 2009.

Bombardelli, C., Artificial spin-up and fragmentation of sub-kilometre asteroids, Acta Astronautica, 65, 1162-1167, 2009.

de Pater, I. and Lissauer, J.J., Planetary Sciences, Cambridge University Press, 2001.

Early, J.T., Space-based Solar Shield to Offset Greenhouse Effect, JBIS, 42, 567-569, 1989.

Govindasamy, B. and Caldeira, K., Geoengineering Earth's radiation balance to mitigate $CO_2$-induced climate change, Geophysical Research Letters, 27, 2141-2144, 2000.

Govindasamy, B., Caldeira, K. and Duffy, P.B., Geoengineering Earth's radiation balance to mitigate climate change from a quadrupling of $CO_2$, Global and Planetary Change, 37, 157-168, 2003.

Harris, A.W., The Rotation Rates of Very Small Asteroids: Evidence for 'Rubble Pile' Structure, Lunar and Planetary Science, 27, 1996.

IPCC, Contribution of Working Groups I, II and III to the Fourth Assessment Report of the Intergovernmental Panel on Climate Change, Core Writing Team, Pachauri, R.K. and Reisinger, A. (Eds.), IPCC, Geneva, Switzerland. pp 104, 2007.

Kahle, R., Kührt, E., Hahn, G., et al., Physical limits of solar collectors in deflecting Earth-threatening asteroids, Aerospace Science and Technology, 10, 256-263, 2006.

Kellenrode, M., Space physics: an introduction to plasmas and particles in the heliosphere and magnetospheres, Springer, 2004.

Kimura, H. and Mann, I., The electric charging of interstellar dust in the solar system and consequences for its dynamics, The Astrophysical Journal, 499, 454-462, 1998.

Koon, W.S., Lo, M., Marsden, J., et al., Dynamical Systems, the Three-Body Problem and Space Mission Design, Marsden Books, 2006.

Lippmann, M.E., In-space fabrication of thin-film structures, NASA, 1st February, 1972.

Maddock, C. A., On the dynamics, navigation and control of a spacecraft formation of solar concentrators in the proximity of an asteroid. PhD thesis, University of Glasgow, 2010

Mautner, M., A Space-based Solar Screen against Climatic Warming, JBIS, 44, 135-138, 1991.

McInnes, C.R., Space-based geoengineering: challenges and requirements, Proceedings of the Institution of Mechanical Engineers, Part C: Journal of Mechanical Engineering Science, 224, 571-580, 2010.

Melosh, H.J., Nemchinov, I.V. and Zetzer, Y.I., Non-Nuclear Strategies for Deflecting Comets and Asteroids, in: Hazards Due to Comets and Asteroids, Gehrels, T. (Ed), University of Arizona Press, 1994.

Minato, T., Köhler, M., Kimura, H., et al., Momentum transfer to interplanetary dust from the solar wind, A&A, 424, L13-L16, 2004.

Olds, J., Charania, A., Graham, M., et al., The League of Extraordinary Machines: A Rapid and Scalable Approach to Planetary Defense Against Asteroid Impactors, NASA Institute for Advanced Concepts, 30th April, 2004.

Pearson, J., Oldson, J. and Levin, E., Earth rings for planetary environment control, Acta Astronautica, 58, 44-57, 2006.

Sanchez, J.P., Asteroid Hazard Mitigation: Deflection Models and Mission Analysis, University of Glasgow, 2009.

Sanchez, J.P. and McInnes, C., Accessibility of the resources of near Earth space using multi-impulse transfers, Astrodynamics Specialist Conference, Toronto, Ontario, Canada, AIAA, 2010.

Sanchez, J.P. and McInnes, C., Asteroid Resource Map for Near-Earth Space, Journal of Spacecraft and Rockets, 48, 153-165, 2011.

Shepherd, J., Caldeira, K., Cox, P. et al., Geoengineering the climate, Report of Royal Society working group of geo-engineering, Royal Society, London, 2009.

Schaub, H. and Junkins, J.L., Analytical Mechanics of Space Systems, AIAA, 2003.

Struck, C., The feasibility of shading the greenhouse with dust clouds at the stable lunar Lagrange points, JBIS, 60, 82-89, 2007.

Wagner, M., Interaction of Interplanetary Dust Particles with magnetic clouds and their further orbital evolution, Christian-Albrechts-Universität zu Kiel, 2007.

Wilck, M. and Mann, I., Radiation pressure forces on "typical" interplanetary dust grains, Planetary and Space Science, 44, 493-499, 1996.

| Method | Complexity | Reliability | Cloud Fit | Efficiency |
|---|---|---|---|---|
| Solar Collector | High | Low | Low | Medium |
| Mass Driver | Medium | High | Medium | High |
| Spin Fragmentation | Medium | Medium | Low | Low |

Table 2: Comparison of different cloud generation methods based on the engineering considerations discussed in this section.